Journal of Intelligent & Robotic Systems (2020) 99:79–90
https://doi.org/10.1007/s10846-019-01109-8

Compliance Control for Robot Manipulation in Contact with a Varied Environment Based on a New Joint Torque Controller

Yunfei Dong[1] · Tianyu Ren[1] · Dan Wu[1] · Ken Chen[1]

Received: 30 January 2019 / Accepted: 26 September 2019 / Published online: 2 January 2020

Abstract
Compliance control is required in the applications of robots for assembling, grinding, polishing and human-robot interface, which needs both position control and force control of robots. The impedance control based on joint torque servo is a promising and practical method to realize compliance control in industrial applications. The performance of a joint torque servo controller is thus crucial to the success of compliance control. However, both nonlinear friction torque of the joint motor and varied dynamics of environmental contact during manipulation increase control difficulty greatly. This paper focuses on the compliance control problem and presents a new joint torque servo controller which is a cascading structure including an inner velocity feedback loop and an outer torque control loop. Due to the high signal-to-noise ratio of the motor velocity, an extended state observer is designed to effectively estimate and compensate for the motor friction torque, varied dynamics of environmental contact and other unknown disturbance. And benefiting from the introduction of the efficient and powerful velocity inner loop, the new torque controller performs very well not only in the rigid but also elastic contact environment. Then a standard PD controller is designed in the outer torque loop to produce the control law. Based on the satisfactory joint torque controller, a simplified impedance control algorithm is designed to achieve the force control. Experiments with three other joint torque controllers on a robot manipulator are conducted to demonstrate the proposed joint torque method and the overall force control framework. These results show the proposed joint torque controller can reduce the steady-state error from 3.07 Nm to 0.21 Nm which indicates the joint actuator friction can be eliminated by more than 99%. And a substantial improvement can also be observed in the experiments of force control based on the new joint torque controller.

Keywords Joint torque control · Force impedance control · Active disturbance rejection control · Varied environment

1 Introduction

Generally, traditional industrial robots are based on pure positon control and have successfully been applied to specific tasks, where the interaction forces between the manipulator and its environment are negligible, such as spray-painting, welding and palletizing. In recent years, the demand of applying a force control technique is greatly increasing; typical examples are assembling, grinding, polishing and human-robot interface [1, 2].

The impedance control based on accurate control of joint torque is a promising approach for robots to achieve high-performance compliance control [3–6]. However the actuator nonlinearity, especially the motor friction and joint torsional flexibility (mainly produced by the most commonly used harmonic drive), deteriorates the output torque behavior of the joint actuator [7–9]. Direct-driver actuators without reducers seem potential for robot actuators to produce accurate joint torques [10], however, the direct drive motor is generally much bulkier than the commonly used actuator consisting of a servo motor with a reducer for the same output torque [11].

On the other hand, some researchers developed the inner-loop joint torque sensing and control technology [12]. Joint torsion torque sensors are designed and then mounted on the joints of the arm to measure the reducer output torques which are used as feedback to realize close-loop joint torque control. In previous work, only simple feedback control laws are used in the close-loop joint torque control system, i.e. simple PID feedback control [13–15]. Pfeffer et al have designed a digital nonlinear compensator for the joint torque feedback control of the third joint of a PUMA 500 based on the dynamic model including accurate modelling of the flexibility, which can reduce the effective friction torque by 97% when the link is immobilized [16].

✉ Dan Wu
wud@tsinghua.edu.cn

[1] State Key Laboratory of Tribology, Department of Mechanical Engineering, Tsinghua University, Beijing, China

Albu-Schäffer and Hirzinger [17] have proposed a globally stable state feedback controller with the idea of remaining the system passivity which can provide joint torque control and has been implemented on the DLR's lightweight robot (the predecessor of KUKA LBR iiwa) [18, 19] and the torque controlled humanoid robot TORO [20]. The globally stable state feedback controller is actually a PD controller with the input feedforward which can be interpreted as a scaling of the apparent motor inertia by model-based parameter setting. This research and the commercial success of KUKA LBR iiwa bring much influence not only in academic communities but also in industrial applications; however, the motor friction is not considered explicitly in the analysis of robot dynamics and cannot be eliminated well by the torque controller. Then Tien et al [21] have designed a friction observer for the DLR medical robot arm and increased the positioning accuracy and the performance of torque control. Hur et al [22] have used a time-delay control (TDC) method to control the joint torque by estimating and eliminating the nonlinear friction and other unknown disturbance. TDC method is actually a PD controller with a delay control term added, which does not need the identification of actuator dynamic model; however it is not enough to compensate for the motor friction by using only TDC method.

Kawai et al have proposed an integral-proportional differential (I-PD) joint torque control method based on a resonance ration control to suppress the vibration duo to joint flexibility [23] and then an improved pseudo I-PD torque controller using load-side torque observer with torsion torque sensor has been proposed in order to improve the back-drivability of the geared motor [24]. However, only a single motor is studied and the torque control performance is not specified by experiments and careful parameter tuning is needed in these two methods which are not easy. In addition, some joint torque controllers are designed just as part of the position control to improve the motion tracking performance, for example, the computed-torque-based joint torque controller by using state feedback law proposed by Tian and Goldenberg [25] and the singular-perturbation-based joint torque controller proposed by Ott et al [26]; however, these joint torque controllers are not designed for pure joint torque control or robot force control and hence corresponding performance are not researched or presented.

It is obvious that the existing joint torque control methods either are improvement to the simple PID controller or require accurate dynamic model of the plant. In most researches, the torque controllers are implemented on the single-joint manipulator or only one joint of the robot manipulator and few researches involve the robot force control by applying the joint torque controllers. The authors have proposed an efficient and simple joint torque controller based on the active disturbance rejection control (ADRC) [27, 28]. This method uses a linear extended state observer (ESO) [29, 30] to estimate and compensate for the motor friction and other unknown disturbance without explicit modeling of the plant or perturbations. The ADRC based joint torque controller can track the reference torque signals very well when contact environment is rigid and then it is implemented on a seven-DOF dexterous collaborative robot arm (DCRA) to realize robot force control by embedding this controller into the impedance control framework. Later study and experiments show that the ADRC joint torque controller needs further improvement when the contact environment is elastic.

The purpose of this paper is to provide a simple and effective force control method based on a novel joint torque controller which provides high performance in not only rigid but also elastic contact environment. The parameter adjusting methods of this controller are convenient and proved in practical application. The main idea is to include an inner ADRC velocity feedback loop in the outer PD torque loop to improve the robustness and accuracy with respect to the environment stiffness. Accurate dynamic model of joint actuators and environment stiffness knowledge are not required by the joint torque control algorithm. Moreover, in order to realize robot force control, a simplified impedance control framework based on the excellent torque controller is designed and the overall proposed control approach is very simple so that it has been easily implemented on the real control systems of the DCRA. The experimental results verify the effectiveness and advantage of the proposed joint torque controller compared with other three methods, and the substantial improvement in force control has been achieved.

This paper is organized as follows: Section 2 introduces the models of the robot and joint actuators. Section 3 describes the cascaded torque controller with ADRC velocity inner loop. Then a simplified impedance algorithm based on the designed joint torque controller is provided for robot force control in Section 4. Section 5 presents the experimental results of joint torque control and robot force control. In these results, the controller performance of the proposed method is exemplified by comparing with other three torque control methods. Finally, conclusions are given in Section 6.

2 Joint Torque Sensor Based System

The Dexterous Collaborative Robot Arm (DCRA) as shown in Fig. 1 is our new 7-DOF robot manipulator under development, which incorporates a lot of advanced designs for being a new generation of collaborative robots [31, 32]. Every joint of DCRA is actuated by the AC Servo Actuator of HarmonicDrive which is an integration of servo motor, encoder and harmonic reducer. And the joint torque sensor is installed at the load side of each actuator to measure the joint torsion torque directly. A PC-based controller is used to control the robot via the EtherCAT bus directly which makes the

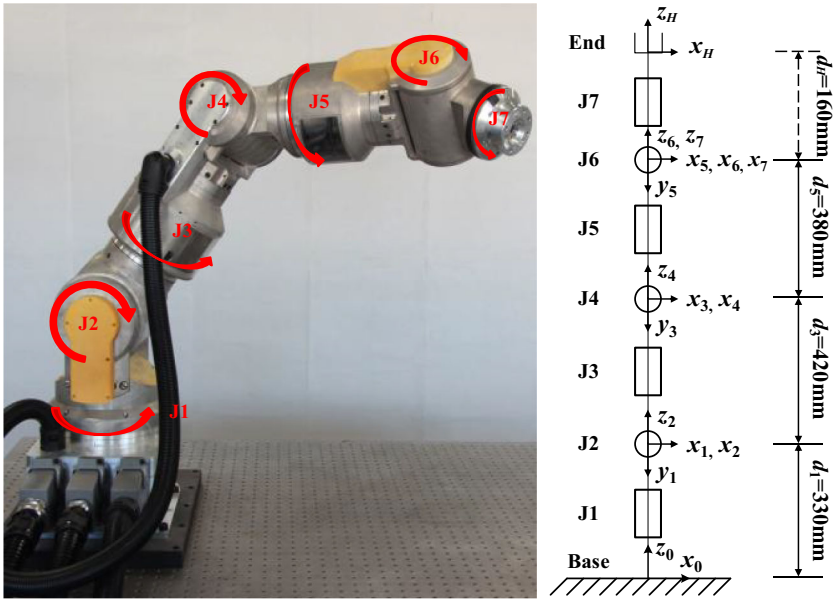

Fig. 1 The 7-DOF dexterous collaborative robot arm (DCRA) and its D-H model

testing and validating of new control algorithms much more easily.

2.1 Dynamic Equation of Robot Manipulators

The dynamic model of an n-degrees-of-freedom robot manipulator is usually expressed in joint space coordinates as,

$$D(q)\ddot{q} + C(q,\dot{q})\dot{q} + g(q) = \tau - \tau_e \tag{1}$$

where the $n \times 1$ vectors $q, \dot{q}, \ddot{q}$ are the joint angle, velocity and acceleration, respectively, $D(q)$ is the $n \times n$ inertia matrix, $C(q,\dot{q})\dot{q}$ is the n-vector torques containing coriolis and centrifugal torques, and $g(q)$ represents n-vector gravitational torques. τ is the $n \times 1$ vector of joint output torque measured by the joint torque sensor, and τ_e is the $n \times 1$ vector of external torque acting on the robot joint which is produced by the contact force between the manipulator and the environment.

2.2 Modeling of the Joint Actuator

Figure 2 shows the typical model of a flexible robot joint actuator as proposed by Spong [33]:

$$\begin{aligned} \tau_m - \tau_f &= D_m\ddot{q}_m + B_m\dot{q}_m + \tau \\ \tau &= K_m(q_m - q) \end{aligned} \tag{2}$$

where τ_m and τ_f are the motor torque and friction respectively; q and q_m represent the link side and motor side angular positions respectively and D_m, B_m, K_m are the motor rotor inertia, motor damping and joint stiffness respectively.

In previous research of the authors, the motion of a robot link q is seen as a source disturbance from the robot-environment system acting on the joint actuator [28]. However in the applications such as grinding and polishing, the robot keeps contact with workpieces. Modeling of the robot-environment contact advances the design of the joint torque controller for better performance. Considering the grinding and polishing application conditions, the robot-environment contact can be modelled as inertia spring damping system and described by

$$\tau = D_l\ddot{q} + B_e\dot{q} + B_e\dot{q} + K_e q \tag{3}$$

where D_l, B_e, K_e are the link inertia, environment contact damping and stiffness respectively. Figure 3 illustrates the derived block diagram of the joint actuator taking account of the robot-environment contact, in which v_m represents the motor velocity.

The transfer function of the joint actuator plant from $\tau_m(s)$ to $\tau(s)$ in Fig. 3 is derived as,

$$Gp = \frac{K_m(D_l s^2 + B_e s + K_e)}{a_4 s^4 + a_3 s^3 + a_2 s^2 + a_1 s + a_0} \tag{4}$$

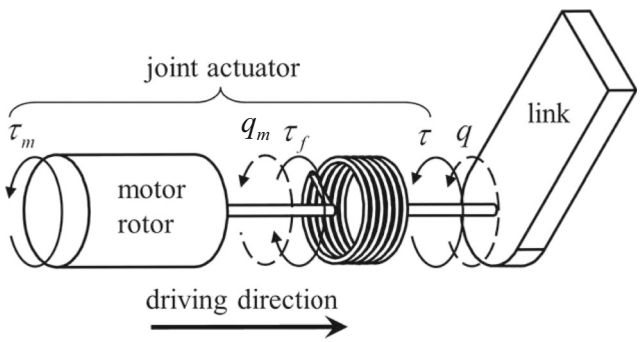

Fig. 2 Schematic model and block diagram of a flexible joint actuator

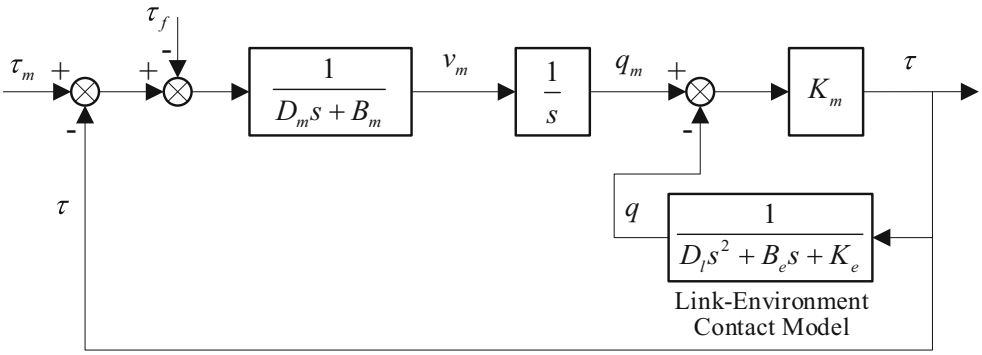

Fig. 3 Block diagram of the joint actuator taking account of the robot-environment contact

where

$$a_4 = D_m D_l$$
$$a_3 = B_m D_l + B_e D_m$$
$$a_2 = B_e B_m + D_l K_m + D_m K_e + D_m K_m$$
$$a_1 = B_e K_m + B_m K_e + B_m K_m$$
$$a_0 = K_m K_e$$

And the friction torque τ_f is seen as the disturbance. Eq. (4) describes a fourth-order system of the plant which is difficult to control well by a single torque feedback loop. It is noticed that when the contact is rigid, i.e. $K_e \to +\infty$, it would be reduced to a second-order system as,

$$Gp = \frac{K_m}{D_m s^2 + B_m s + K_m} \tag{5}$$

It is observed is that when the robot-environment contact is varied in the situations such as the robotic grinding and polishing, the system described by Eq. (4) is time-varying, which will greatly increase control difficulty. Thus more efficient and robust control algorithms are demanded.

In addition, motor friction τ_f is significant disturbance whose influence is presented in our previous report [28] through a static loading experiment in the Joint 4. The maximum static friction is about 22 Nm which is the same order of magnitude as the demanded joint torque. More seriously, the Coulomb friction has strong nonlinearity in low velocity zone, which is hardly modelled accurately and considered as the major source of nonlinear disturbance in the problem of the joint torque control. Therefore, in this paper the friction disturbance is not modelled, and instead, an observer is used to estimate and compensate for it to decrease its negative effects in real time.

3 Design of Joint Torque Controller

In this section, we present our cascaded joint torque controller architecture which is illustrated in Fig. 4. In the following the designs of inner ADRC velocity loop and outer PD torque loop are introduced respectively.

3.1 Cascaded Torque Controller with Inner Velocity Loop

It is noted that during the robotic grinding or polishing, the joint velocities are generally known from preliminary motion planning, but the robot-environment contact damping and stiffness are varied. This means that both feedforward and robustness should be considered in the joint torque control framework. Figure 4 presents a new design strategy, in which an active disturbance rejection based velocity controller is cascaded into the commonly used PD torque controller, and a velocity feedforward is involved. Such a combined controller has potential to achieve better robustness and high accuracy of torque control.

In Fig. 4, τ_d is the desired control torque, v_c and v_d are the output velocity of the torque outer loop and the desired velocity of the velocity inner loop respectively and v_{ff} is the feedforward velocity which can be obtained from preliminary motion planning.

3.2 Design of the Inner ADRC Velocity Loop

Considering the robot-environment contact dynamics variation during robot manipulation and nonlinear joint friction, the active disturbance rejection control (ADRC) concept is thus used to improve the joint velocity control performance.

The method of ADRC is used in the inner velocity loop to track velocity. In the ADRC framework, the ESO proposed by Han [30] has been proved the abilities to track different types of unknown disturbance in real time and compensate for them [34]. And the magnitude of the ESO's errors monotonically decrease with the observer bandwidth [35]. Due to the high signal-to-noise ratio of velocity, the ESO's bandwidth can be set very high.

To design the ADRC based joint velocity control loop, basic knowledge of the plant is required. In Fig. 3, the transfer function from the motor torque τ_m to the motor velocity v_m can be derived as,

$$G_{p(\tau_m \to v_m)} = \frac{D_l s^3 + B_e s^2 + (K_m + K_e)s}{a_4 s^4 + a_3 s^3 + a_2 s^2 + a_1 s + a_0} \tag{6}$$

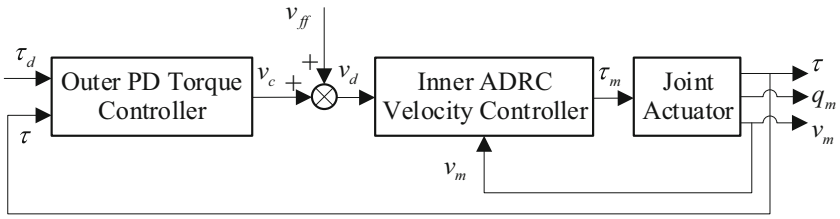

Fig. 4 Block diagram of the cascaded torque controller with inner velocity loop

wherein, the meanings of all parameters are the same as those in Eq. (4). Eq. (6) indicates that the joint actuator is a fourth-order plant and the relative order of the numerator and denominator is one. Hence the corresponding differential equation of the plant can be expressed as,

$$\dot{v}_m = f + \frac{D_l}{a_4}\tau_m = f + \frac{1}{D_m}\tau_m = f + b\tau_m \tag{7}$$

where f is donated as the total disturbance, including the effect of both internal dynamics and external disturbance. It's not necessary to model the disturbance f in ADRC, because the ESO can estimate the value of f in real time. $b = 1/D_m$ is a system parameter and it can be calculated from the plant information.

The basic idea of the ESO is to use an augmented the state space to include the unknown disturbance f as an additional state. Then, Eq. (7) can be expressed in the augmented state space form as,

$$\begin{cases} \dot{x}_1 = x_2 + b\tau_m \\ \dot{x}_2 = \dot{f} \\ y = x_1 \end{cases} \quad \text{with} \quad \begin{cases} x_1 = v_m \\ x_2 = f \end{cases} \tag{8}$$

Now the linear version of a second-order ESO can be designed to estimate the augmented plant states.

$$\begin{cases} e_o = z_1 - v_m \\ \dot{z}_1 = z_2 - \beta_1 e_0 + b_o\tau_m \\ \dot{z}_2 = -\beta_2 e_o \end{cases} \tag{9}$$

where, b_0 is the estimated value of the actual system parameter b, e_o is the estimation error of the motor velocity v_m, and $\beta_1\beta_2$ are the gains of the ESO which are chosen by a pole-placement method [36] such that all the observer eigenvalues are located at $-\omega_0$.

$$\beta_1 = 2\omega_0, \beta_2 = \omega_0^2 \tag{10}$$

Now if the observer is well-tuned, the outputs of ESO z_1 and z_2 can closely track x_1 and x_2 i.e.v_m and f respectively. Here, an assumption that f is bounded or its time derivative is bounded is required to ensure that the estimation errors are bounded [37]. And this assumption is reasonable for the real robot, because the discontinuity of the disturbance will be 'smoothed' by the actual mechanical structures and electrical components.

As the observer output z_2 is the estimation of the disturbance f, the control law can be designed as follows,

$$\tau_m = \tau_c - \frac{z_2}{b_0} \tag{11}$$

where τ_c is the output signal from a simple feedback controller. Then the original plant (6) will be reduced to a single-integral system,

$$\dot{v}_m = f + b\tau_m \approx z_2 + b_0\left(\tau_c - \frac{z_2}{b_0}\right) = b_0\tau_c \tag{12}$$

which can be easily controlled by a proportional controller, and the control law is,

$$\tau_c = k_{Ap}(v_d - z_1) \tag{13}$$

k_{AP} is the gain of the feedback controller of the ADRC and can be tuned just as a regular P controller. Now, the active disturbance rejection controller has been established for the velocity inner loop of the robot joint torque servo and its configuration is shown in Fig. 5.

According to the pole placement method, the gain of k_{AP} is chosen as ω_c which places the close-loop pole at $-\omega_c$. In the ADRC, only ω_0 and ω_c need to be tuned, which are denoted as the bandwidths of the ESO and the controller [36]. Generally, higher bandwidth can provide better tracking performance and reduce the apparent motor inertia viewed from the actuator output end. However, higher bandwidth will lead to larger ripple threshold for the control signal and make the system more sensitive to the sensor noises. The method of adjusting parameters proposed in Gao [36] can be served as reference.

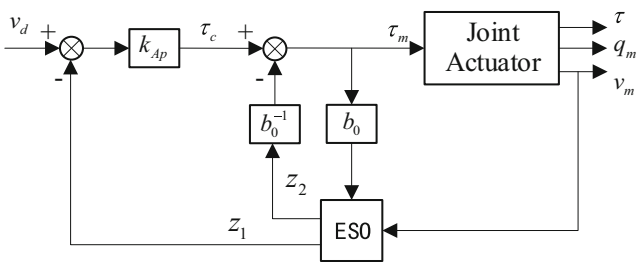

Fig. 5 Configuration of the proposed ADRC for the velocity inner loop of the robot joint torque servo

3.3 Design of the Outer PD Torque Loop

The outer torque feedback loop is designed as a simple proportional and differential controller. To reduce the noise disturbance of joint torque sensor and obtain the torque differential signal, a simple and efficient tracking differentiator (TD) [30] is applied to filter the torque signal and calculate its differential. The tracking differentiator can be expressed as,

$$\begin{cases} f_h = fhan\left(\overline{\tau}-\tau, \dot{\tau}, r_0, h_0\right) \\ \overline{\tau} = \overline{\tau} + h\dot{\tau} \\ \dot{\tau} = \dot{\tau} + hf_h \end{cases} \tag{14}$$

where $\overline{\tau}$ and $\dot{\tau}$ is the filtered joint torque and its differential respectively, h is the sampling period of joint torque sensors, and fhan(x_1, x_2, r_0, h_0) is a nonlinear function employed in TD,

$$\begin{cases} d = r_0 h_0 \\ d_0 = h_0 d \\ y = x_1 + h_0 x_2 \\ a_0 = \sqrt{d^2 + 8r|y|} \\ a = \begin{cases} x_2 + \dfrac{(a_0-d)}{2}\text{sign}(y), & |y| > d_0 \\ x_2 + \dfrac{y}{h_0}, & |y| \le d_0 \end{cases} \\ \text{fhan}(x_1, x_2, r_0, h_0) = -\begin{cases} r\,\text{sign}(a), & |a| > d \\ r\dfrac{a}{d}, & |a| \le d \end{cases} \end{cases} \tag{15}$$

The parameter r_0 is called the speed factor which approximately decides the corner frequency of TD (i.e., $\omega_{TD} \approx 1.14 \times \sqrt{r_0}$) and h_0 is the filter factor of TD which is set bigger than the sampling period h to reduce the differential noise stronger.

The control law of the outer torque loop can be written as,

$$v_c = k_p\left(\tau_d - \overline{\tau}\right) + k_d\left(\dot{\tau}_d - \dot{\tau}\right) \tag{16}$$

wherein, v_c is the output velocity of the torque outer loop and τ_d is the commanded torque and $\dot{\tau}_d$ is the derivative of the commanded torque if it is also provided by the upper controller in ideal situation; otherwise the commanded torque derivative can be calculated by a differentiator or just be set as zero in consideration of low change rate of the command torque in general applications of joint torque control.

Then the velocity feedforward v_{ff} is introduced for the velocity inner loop,

$$v_d = v_c + v_{ff} \tag{17}$$

Finally the complete cascaded joint torque controller with the inner ADRC velocity loop and the outer PD torque loop has been established which can be called as PD-ADRC method for short and its architecture is illustrated in Fig. 6.

4 Design of the Torque-Based Impedance Control

Because the proposed joint torque controller can provide satisfactory torque servo performance, a simpler and more intuitive torque-based impedance control structure than that presented in [2, 38] is developed in the paper. The end-effector velocities in Cartesian space $\dot{X}$ are related to the joint velocities $\dot{q}$, i.e.,

$$\dot{X} = J(q)\dot{q} \tag{18}$$

where J is the $6 \times n$ Jacobian matrix which represents the relationship between virtual end-effector displacements and virtual joint displacements. On the other hand, the relationship between the actuator forces F in Cartesian space and the joint torques τ can expressed as,

$$\tau = J(q)^T F \tag{19}$$

By differentiating the Eq. (18), the Cartesian accelerations X can be derived as,

$$\ddot{X} = J(q)\ddot{q} + \dot{J}\dot{q} \tag{20}$$

Then the joint velocities $\dot{q}$ and accelerations q can be represented in Cartesian space coordinates by the relationship,

$$\begin{aligned} \dot{q} &= J(q)^{-1}\dot{X} \\ \ddot{q} &= J(q)^{-1}\left(\ddot{X} - \dot{J}\dot{q}\right) = J^{-1}\left(\ddot{X} - \dot{J}J^{-1}\dot{X}\right) \end{aligned} \tag{21}$$

Substituting Eq. (19) and Eq. (21) into the robot dynamic model in joint space Eq. (1) yields,

$$DJ^{-1}\left(\ddot{X} - \dot{J}J^{-1}\dot{X}\right) + CJ^{-1}\dot{X} + g = J^T F - J^T F_e \tag{22}$$

Then the robot dynamic model in Cartesian space is derived as,

$$D^*\ddot{X} + C^*\dot{X} + g^* = F - F_e \tag{23}$$

where,

$$\begin{aligned} D^* &= J^{T-1}DJ^{-1}, C^* = J^{T-1}CJ^{-1} - J^{T-1}DJ^{-1}\dot{J}J^{-1}, g^* \\ &= J^{T-1}g \end{aligned} \tag{24}$$

and F_e are the exerted forces of the robot manipulator on environment.

Now the torque-based impedance control structure is designed as shown in Fig. 7. The torque-based impedance control law is,

$$\tau_d = J^T\left(K(X_r - X) + B\left(\dot{X}_r - \dot{X}\right)\right) + \tau_{dyn} \tag{25}$$

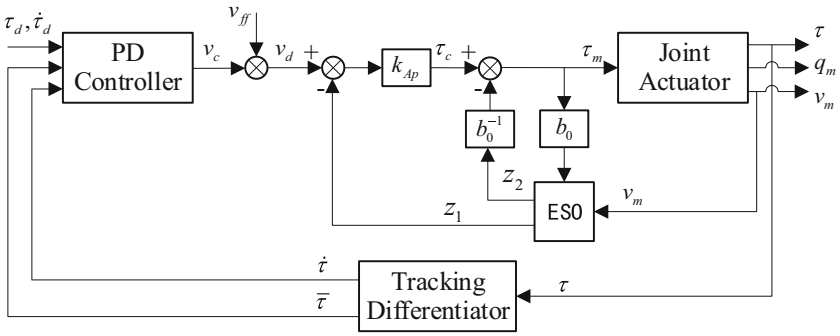

Fig. 6 Architecture of the developed cascaded joint torque controller with inner ADRC velocity loop and outer PD torque loop (PD-ADRC method)

wherein, τ_d are the commanded torques for the joint torque controller proposed in this paper, K, B are $n \times n$ symmetric positive-definite desired stiffness and damping gain matrices, respectively, and X_r is the reference end-point trajectory. τ_{dyn} are feedforward torques of dynamic model which can be expressed as,

$$\tau_{dyn} = \hat{D}(q)q + \hat{C}(q,\dot{q})\dot{q} + \hat{g}(q) \tag{26}$$

where, $\hat{D}, \hat{C}, \hat{g}$ are the estimations of the actual D, C, g, which can be obtained by the method of robot parameter identification.

Converting the torque-based impedance control law of Eq. (25) into the Cartesian space as above, which can be expressed as,

$$F_d = K(X_r - X) + B(\dot{X}_r - \dot{X}) + \hat{D}^*\ddot{X} + \hat{C}^*\dot{X} + \hat{g}^*$$

with

$$\hat{D}^* = J^{T-1}\hat{D}J^{-1}, \hat{C}^* = J^{T-1}\hat{C}J^{-1} - J^{T-1}\hat{D}J^{-1}\dot{J}J^{-1}, \hat{g}^* = J^{T-1}\hat{g} \tag{27}$$

The F_d are the commanded forces of the actuator forces F in the torque-based impedance control law. Combining Eq. (23) and Eq. (27) yields the closed-loop tracking error dynamic equation,

$$KE + B\dot{E} - F_e = \Delta D^*\ddot{X} + \Delta C^*\dot{X} + \Delta g^* \tag{28}$$

where

$$\Delta D^* = D^* - \hat{D}^* = J^{T-1}\left(D - \hat{D}\right)J^{-1}$$
$$\Delta C^* = C^* - \hat{C}^* = J^{T-1}\left(C - \hat{C}\right)J^{-1} - J^{T-1}\left(D - \hat{D}\right)J^{-1}\dot{J}J^{-1},$$
$$\Delta g^* = g^* - \hat{g}^* = J^{T-1}(g - \hat{g})$$

And $E = X_r - X$ are the tracking errors of the end-point position. In the ideal case, the robot parameter identification could be accurate, then $\Delta D^* = \Delta C^* = \Delta g^* = 0$; as a consequence the closed-loop robot behavior would satisfies the target impedance relationships,

$$F_e = KE + B\dot{E} \tag{29}$$

To exert the desired contact force, the reference end-point trajectory X_r should be designed based on F_{ed}, X_e, K and K_e, as following,

$$x_r = x_e + \frac{f_{ed}}{k_{eff}} \tag{30}$$

where F_{ed} are the desired force of the actual contact forces F_e, X_e, K_e are the positions and stiffness of the environment, respectively, x_r, x_e, f_{ed} represent elements of X_r, X_e, F_{ed}, respectively, and k_{eff} is the equivalent stiffness of the series structure of the environment and the robot.

$$k_{eff} = \frac{kk_e}{k + k_e} \tag{31}$$

wherein, k and k_e are corresponding elements of K and K_e. Ideally, the environment position and stiffness x_e, k_e are precisely known, therefore it is easy to obtain the reference trajectory x_r from Eqs. (30–31).

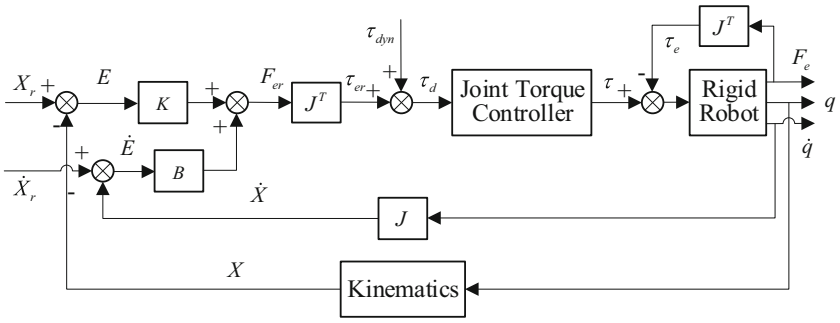

Fig. 7 The control structure for the torque-based impedance control

5 Experiment Results and Comparative Analysis

To illustrate the excellent performance of the cascaded joint torque controller with inner ADRC velocity loop proposed in this paper, several experiments were conducted to compare this method with another three methods including the DLR's State Feedback Controller [17], the time-delay controller (TDC) [22] and the ADRC controller proposed by the authors in previous research [28].

5.1 Joint Torque Control Experiments

Firstly we tested the proposed torque controller with the fourth axis of the 7-DOF manipulator as shown in Fig. 8. The robot presses its end-effector onto a rigid fixture (Fig. 8a) and a fixed surface plate covered with elastic foamed plastic (Fig. 8b) which are used as the rigid and elastic contact environments respectively. Both square waves and harmonic waves are set as the reference joint torque signals and the contact environments of high stiffness and low stiffness are tested respectively.

The performance comparisons of the four methods are shown in Fig. 9 and Fig. 10. All the controllers are tuned with proper gains to give a good performance on response rapidity and steady-state error while keeping the system stable. And the controller parameters remain the same when the environment stiffness changes.

In the high stiffness environment which is basically rigid (see in Fig. 8a), all of the four controllers seem to have good performance. However, when the contact environment has certain elasticity (see in Fig. 8b), the performance of DLR's State Feedback method and TDC method deteriorates. The steady-state error of the DLR's method is large which means it cannot effectively eliminate the system disturbance, the friction mainly. As for the TDC method there always is notable sawteeth when it should have reached stable state. And this notable sawteeth also exists in the research [22].

Four representative step-response characteristics are chosen to compare these four control methods in detail, which is shown in Table 1. t_r, M_p, t_s and e_{ss} represents rise time,. overshoot, settling time within the 2% error band and steady-state error respectively.

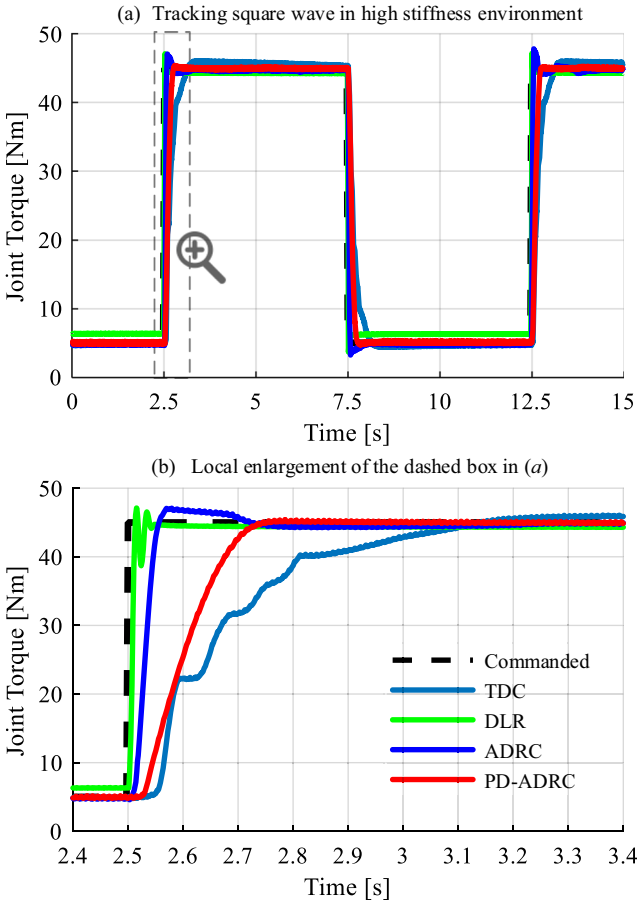

Fig. 9 System responses of the four control methods to square wave input in high stiffness environment

It can be observed that the TDC method needs too long rise time and settling time and the notable sawteeth in elastic environment is unsatisfactory. The DLR's State Feedback method has the best performance in rapidity while has certain overshoot in both rigid and elastic environment and significant steady-state errors in elastic environment which could make the force control not precise enough. Therefore the DLR's State Feedback method could be more applicable to the

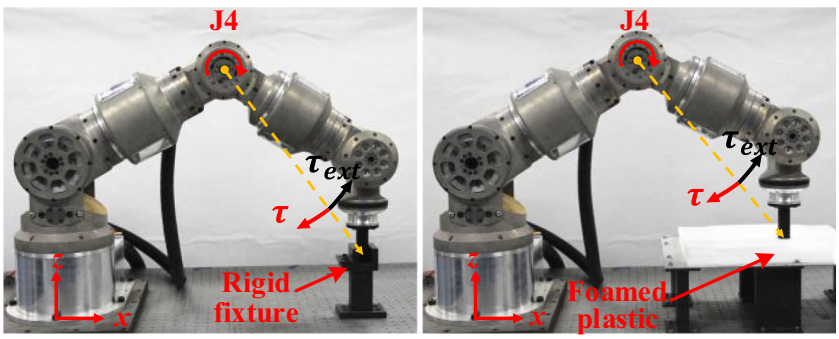

(a) Rigid contact environment (b) Elastic contact environment

Fig. 8 The joint torque control experiments of different environment stiffness

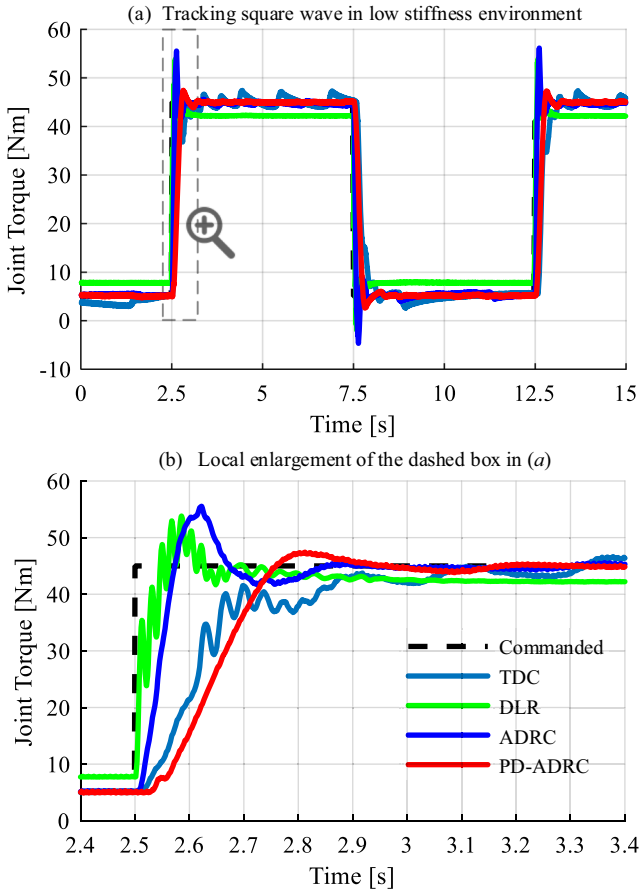

Fig. 10 System response of the four control methods to square wave input in low stiffness environment

applications that need quick response. The ADRC method is better, however its overshoot and steady-state error is bigger than the PD-ADRC method, especially in elastic environment. The PD-ADRC method provides the best tracking accuracy in both rigid environment and elastic environment. Its steady-state errors are 0.17 Nm and 0.22 Nm in rigid and elastic environment respectively and the maximum static friction of this actuator is about 22 Nm, and this indicates the PD-ADRC method can reduce the effective friction by more than 99% in both rigid and elastic environment which is excellent and satisfactory. The disadvantage of the PD-ADRC method is its rising speed is slightly slow, hence it applicable for the force control applications such as polishing and sanding which pay greater attention to the accuracy and smoothness than rapidity. In addition the PD-ADRC method has stronger adaptability than the other methods in different stiffness environments, therefore, it is proved that the new joint torque method proposed in this paper has a good application potential.

Table 1 Step-response characteristics of the four control methods

		TDC	DLR	ADRC	PD-ADRC
High Stiffness	t_r[ms]	346	8	30	142
	M_p	2.5%	5.3%	5.1%	0.8%
	t_s[ms]	617	43	78	203
	e_{ss}[Nm]	0.42	0.58	0.22	0.17
Low Stiffness	t_r[ms]	159	42	49	160
	M_p	6%	22%	26%	6%
	t_s[ms]	∞	∞	302	343
	e_{ss}[Nm]	2.42	2.82	0.69	0.21

The different performances of the four controllers can be analyzed as follows. For the DLR's State Feedback method, it is a PD controller with the input torque feedforward, therefore, the accurately calibrated motor torque constant makes the torque feedforward is accurate when the environment is rigid; however when the environment is elastic, visible motor rotation is need to track the commanded torque, and the nonlinear friction cannot be compensated well because of the limitation of the pure PD controller. For the TDC controller, the existence of the delay term makes the compensation is too high and too low alternately and cannot estimate the nonlinear friction in real-time. Consequently, the TDC controller has poor rapidity and there will be notable sawteeth even it should have reached stable state. In both the ADRC method and the PD-ADRC method, the ESO usually has a much higher bandwidth than the closed-loop system, and small deviation from the reference signal is accumulated in ESO as a disturbance and finally eliminated by the controller [30]. Because the velocity signals have higher signal-to-noise ratio than the torque signal, the ESO in the velocity inner loop can give stronger estimation and compensation of disturbance and bring in smaller steady-state errors.

To illustrate the differences of these four methods more clearly, harmonic waves of different frequencies are set as the reference signals and the environment is elastic as same as the above experiments (see in Fig. 8b). The tracking results are shown in Fig. 11. There are obvious tracking errors in both frequencies for the DLR's State Feedback method, and the lag time of TDC method is close to one fourth cycle when the input frequency increases from 0.1 Hz to 1 Hz. The ADRC method and PD-ADRC method give almost same and much better performance to track the harmonic waves and the tracking accuracy and rapidity are quite good even the bandwidth is up to 1 Hz and the peak-valley value is 40 Nm (from 5 Nm to 45 Nm).

5.2 Torque-Based Impedance Control Experiments

The main purpose of designing the joint torque controller is to achieve the torque based impedance control. Hence, a group of impedance control experiments are conducted to contrast the performance of the four joint control methods in force control applications. The experimental setup is shown in Fig. 12. The robot is commanded to move

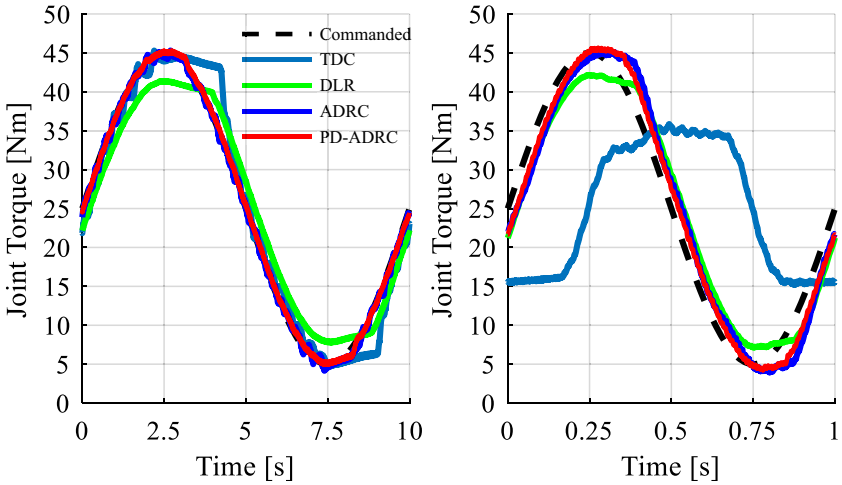

Fig. 11 System response of the four control methods to harmonic wave input of different frequencies in low stiffness environment. Left: 0.1 Hz, Right: 1 Hz

100 mm forth and back in the x direction in about 24 s with the desired force $f_{zd} = -20$N in the z direction which is used to imitate the polishing application. The joint 2, 4, and 6 are used for this task which represent the all three types of actuators used in the DCRA from axis 1 to 6. The contact environment is a flat elastic surface covered with foamed plastic and an ATI six DOFs Force/Torque sensor is installed between the robot and the rubber wheel to measure the contact force accurately. It should be noted that the F/T sensor is just served as monitoring purposes and does not provide any control function.

The results of the contrast experiments using the above four joint torque control methods under the same conditions are shown in Fig. 13 and Table 2. Because the error amplitude of the TDC method is much bigger than the others, its results are not plotted in Fig. 13. It should be noted that, as shown in Fig. 13a, the large deviations of contact force appearing in case of the DLR method around 14 s and 0 s were the actual experimental result and would always happen in repeated experiments. Because the rotation direction of axis 6 need to change from positive to negative around 14 s. The axis 6 remained static unexpectedly for about 2.5 s while the static friction of axis 6 is very large and the DLR method cannot eliminate it very well. As a result there occurred large deviations in the contact force around 14 s as well as 0 s.

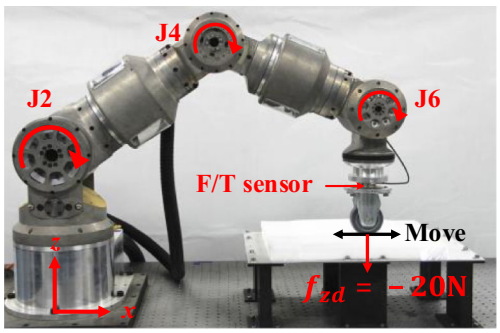

Fig. 12 Torque-based impedance control experiments

It can be obviously observed that the PD-ADRC method provides the best impedance control performance and the force is controlled to within ±11% which is much better than the other three methods. In addition, its larger force errors only occur when the robot accelerates, decelerates and changes the direction of movement, but other than those the force errors are just within ±5% for most of the time and it can be indicated by the mean absolute error of just 0.42 N. As for the position

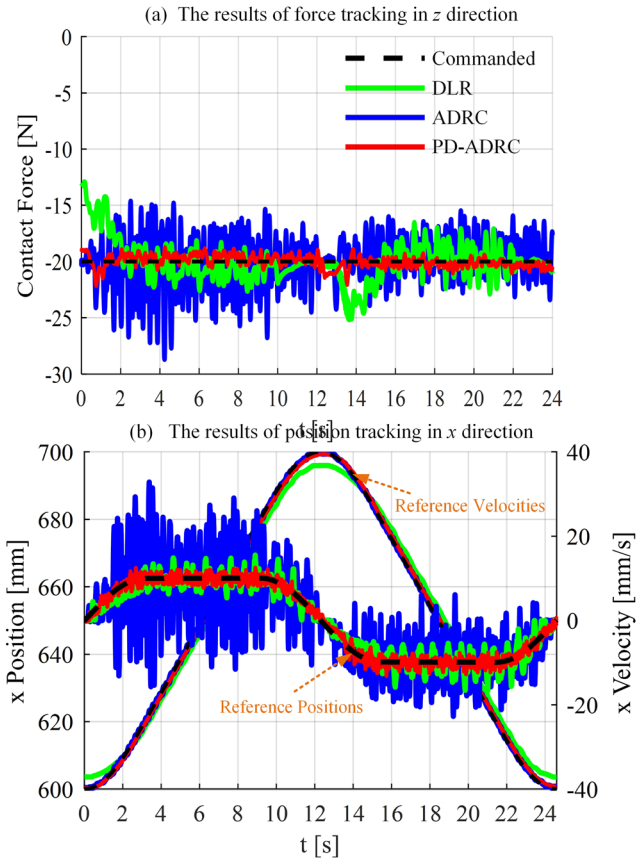

Fig. 13 The comparison results of impedance control experiment based on different joint torque control methods

Table 2 The tracking errors of force, position and velocity in the impedance control experiments based on different joint torque control methods

		TDC	DLR	ADRC	PD-ADRC
Max absolute error	F_z [N]	37.10	7.09	8.71	2.18
	x [mm]	4.97	4.22	1.04	1.39
	v_x [mm/s]	68.48	6.80	25.70	3.34
Mean absolute error	F_z [N]	8.41	1.30	1.76	0.42
	x [mm]	1.48	2.89	0.40	0.92
	v_x [mm/s]	14.47	1.77	5.46	0.70

tracking in x direction, the PD-ADRC method also provides the best comprehensive result, although it has a little bigger error than the ADRC method; however, the velocity using ADRC method waves too widely and the PD-ADRC method gives the best and much better velocity tracking. The velocity fluctuation in x direction not only affects the position accuracy but also disturbs the force tracking in z direction. Due to the inner ADRC velocity loop in PD-ADRC method, it has a natural and powerful ability to suppress the velocity vibration which makes it very suitable for the impedance control to well track the force and position at the same time.

6 Conclusions

A new, simple and practical force control scheme for flexible joint robots is presented in this paper. By adding an inner active disturbance rejection velocity feedback loop in the outer PD torque loop, the proposed joint torque servo controller can effectively track the reference signals while actively estimating and eliminating all disturbance without explicit modeling of the plant or perturbations. The results of contrast experiment show that the proposed joint torque controller provides a substantial reduction of the effective friction by more than 99% in not only rigid but also elastic contact environment which is a greater improvement than the existing methods. On the basis that the closed-loop joint actuators almost become ideal torque sources, a new and simplified impedance control scheme is achieved for the force control of the multi-joint robot. The experiment results showed that the proposed force controller is excellent to achieve the satisfactory force/position tracking under the unknown elastic contact environment, which benefits from the high performance of the new joint torque controller. Moreover, it is remarkable that the complete force control scheme proposed by this paper is easy to implement on robot systems. Future work is to improve the rapidity of the new joint torque controller and to apply the developed force control method to the practical grinding and polishing applications.

References

1. Hogan, N.: Impedance Control: An Approach to Manipulation. In: 1984 American Control Conference. pp. 304–313. IEEE (1984)
2. Jung, S., Hsia, T.C., Bonitz, R.G.: Force tracking impedance control of robot manipulators under unknown environment. IEEE Trans. Control Syst. Technol. **12**(3), 474–483 (2004). https://doi.org/10.1109/TCST.2004.824320
3. Hirzinger, G., Albu-Schaffer, A., Hahnle, M., Schaefer, I., Sporer, N.: On a new generation of torque controlled light-weight robots. In: Proceedings 2001 ICRA. IEEE International Conference on Robotics and Automation (Cat. No.01CH37164). pp. 3356–3363. IEEE (2001)
4. Vallery, H., Veneman, J., van Asseldonk, E., Ekkelenkamp, R., Buss, M., van der Kooij, H.: Compliant actuation of rehabilitation robots. IEEE Robotics Automation Magazine. **15**(3), 60–69 (2008). https://doi.org/10.1109/MRA.2008.927689
5. Focchi, M., Medrano-Cerda, G.A., Boaventura, T., Frigerio, M., Semini, C., Buchli, J., Caldwell, D.G.: Robot impedance control and passivity analysis with inner torque and velocity feedback loops. Control Theory Technol. **14**(2), 97–112 (2016). https://doi.org/10.1007/s11768-016-5015-z
6. Ren, T., Dong, Y., Wu, D., Chen, K.: Learning-based variable compliance control for robotic assembly. J. Mechanisms Robotics. **10**(6), 061008 (2018). https://doi.org/10.1115/1.4041331
7. Hashimoto, M., Horiuchi, T., Kiyosawa, Y., Hirabayashi, H.: The effects of joint flexibility on robot motion control based on joint torque positive feedback. In: Proceedings. 1991 IEEE International Conference on Robotics and Automation. pp. 1220–1225. IEEE (1991)
8. Townsend, W., Salisbury, J.: The Effect of coulomb friction and stiction on force control. In: Proceedings. 1987 IEEE International Conference on Robotics and Automation. pp. 883–889. IEEE (1987)
9. Ren, T., Dong, Y., Wu, D., Chen, K.: Design of Direct Teaching Behavior of collaborative robot based on force interaction. J. Intell. Robot. Syst. **96**, 83–93 (2019). https://doi.org/10.1007/s10846-019-00986-3
10. Hollerbach, J., Hunter, I., Lang, J., Umans, S., Sepe, R., Vaaler, E., Garabieta, I.: The McGill/MIT direct drive motor project. In: [1993] Proceedings IEEE International Conference on Robotics and Automation. pp. 611–617. IEEE (1993)
11. Hunter, I.W., Hollerbach, J.M., Ballantyne, J.: A comparative analysis of actuator technologies for robotics. Robot. Rev. **2**, 299–342 (1991)
12. Albu-Schaffer, A., Eiberger, O., Grebenstein, M., Haddadin, S., Ott, C., Wimbock, T., Wolf, S., Hirzinger, G.: Soft robotics. IEEE Robotics Automation Magazine. **15**(3), 20–30 (2008). https://doi.org/10.1109/MRA.2008.927979
13. Luh, J., Fisher, W., Paul, R.: Joint torque control by a direct feedback for industrial robots. IEEE Trans. Autom. Control. **28**(2), 153–161 (1983). https://doi.org/10.1109/TAC.1983.1103215
14. Wu, C.: Compliance control of a robot manipulator based on joint torque servo. Int. J. Robot. Res. **4**(3), 55–71 (1985). https://doi.org/10.1177/027836498500400305
15. Wu, C. H, Paul, R.P.: Manipulator compliance based on joint torque control. In: 1980 19th IEEE Conference on Decision and Control including the Symposium on Adaptive Processes. pp. 88–94. IEEE (1980)
16. Pfeffer, L.E., Khatib, O., Hake, J.: Joint torque sensory feedback in the control of a PUMA manipulator. IEEE Trans. Robot. Autom. **5**(4), 418–425 (1989). https://doi.org/10.1109/70.88056
17. Albu-Schäffer, A., Hirzinger, G.: A globally stable state feedback controller for flexible joint robots. Adv. Robot. **15**(8), 799–814 (2001). https://doi.org/10.1163/156855301317198133

18. Albu-Schaffer, A., Ott, C., Hirzinger, G.: A passivity based Cartesian impedance controller for flexible joint robots - part II: full state feedback, impedance design and experiments. In: IEEE International Conference on Robotics and Automation, 2004. Proceedings. ICRA'04. 2004. pp. 2666–2672. IEEE (2004)
19. Ott, C., Albu-Schaffer, A., Kugi, A., Stamigioli, S., Hirzinger, G.: A passivity based Cartesian impedance controller for flexible joint robots - part I: torque feedback and gravity compensation. In: IEEE International Conference on Robotics and Automation, 2004. Proceedings. ICRA '04. 2004. pp. 2659–2665. IEEE (2004)
20. Englsberger, J., Werner, A., Ott, C., Henze, B., Roa, M.A., Garofalo, G., Burger, R., Beyer, A., Eiberger, O., Schmid, K., Albu-Schäffer, A.: Overview of the torque-controlled humanoid robot TORO. In: 2014 IEEE-RAS International Conference on Humanoid Robots. pp. 916–923. IEEE (2014)
21. Tien, L.L., Albu-Schaffer, A., Luca, A.D., Hirzinger, G.: Friction observer and compensation for control of robots with joint torque measurement. In: 2008 IEEE/RSJ International Conference on Intelligent Robots and Systems. pp. 3789–3795. IEEE (2008)
22. Hur, S.M, Kim, S.K., Oh, Y., Oh, S.R.: Joint torque servo of a high friction robot manipulator based on time-delay control with feed-forward friction compensation. In: 2012 IEEE RO-MAN: The 21st IEEE International Symposium on Robot and Human Interactive Communication. pp. 37–42. IEEE (2012)
23. Kawai, Y., Yokokura, Y., Ohishi, K., Saito, K., Shimamoto, A.: Equivalence of resonance ratio and I-PD controllers in zero stiffness torque control for soft robot. In: IECON 2015 - 41st Annual Conference of the IEEE Industrial Electronics Society. pp. 001424–001429. IEEE (2015)
24. Kawai, Y., Yokokura, Y., Ohishi, K., Saito, K., Shimamoto, A.: High back-drivable pseudo I-PD torque control using load-side torque observer with torsion torque sensor. In: 2016 IEEE 14th International Workshop on Advanced Motion Control (AMC). pp. 167–172. IEEE (2016)
25. Tian, L., Goldenberg, A.A.: Robust adaptive control of flexible joint robots with joint torque feedback. In: Proceedings of 1995 IEEE International Conference on Robotics and Automation. pp. 1229–1234 (1995)
26. Ott, C., Albu-Schaffer, A., Hirzinger, G.: Comparison of adaptive and nonadaptive tracking control laws for a flexible joint manipulator. In: IEEE/RSJ International Conference on Intelligent Robots and Systems. pp. 2018–2024. IEEE (2002)
27. Ren, T., Dong, Y., Wu, D., Wang, G., Chen, K.: Joint Torque Control of a Collaborative Robot Based on Active Disturbance Rejection With the Consideration of Actuator Delay. In: ASME 2017 International Mechanical Engineering Congress and Exposition. p. V04AT05A010. American Society of Mechanical Engineers (2017)
28. Ren, T., Dong, Y., Wu, D., Chen, K.: Impedance control of collaborative robots based on joint torque servo with active disturbance rejection. Industrial Robot: the international journal of robotics research and application. (2018). https://doi.org/10.1108/IR-06-2018-0130
29. Gao, Z.: Active disturbance rejection control: a paradigm shift in feedback control system design. In: 2006 American Control Conference. pp. 2399–2405. IEEE (2006)
30. Han, J.: From PID to active disturbance rejection control. IEEE Trans. Ind. Electron. **56**(3), 900–906 (2009). https://doi.org/10.1109/TIE.2008.2011621
31. Ren, T., Dong, Y., Wu, D., Chen, K.: Collision detection and identification for robot manipulators based on extended state observer. Control. Eng. Pract. **79**, 144–153 (2018). https://doi.org/10.1016/j.conengprac.2018.07.004
32. Dong, Y., Ren, T., Chen, K., Wu, D.: An efficient robot payload identification method for industrial application. Ind. Robot. **45**(4), 505–515 (2018). https://doi.org/10.1108/IR-03-2018-0037
33. Spong, M.W.: Modeling and Control of Elastic Joint Robots. J. Dyn. Syst. Meas. Control. **109**(4), 310–319 (1987). https://doi.org/10.1115/1.3143860
34. Yoo, D., Yau, S.S.-T., Gao, Z.: Optimal fast tracking observer bandwidth of the linear extended state observer. Int. J. Control. **80**(1), 102–111 (2007). https://doi.org/10.1080/00207170600936555
35. Zhou, W., Shao, S., Gao, Z.: A stability study of the active disturbance rejection control problem by a singular perturbation approach. Appl. Math. Sci. **3**(10), 491–508 (2009)
36. Gao, Z.: Scaling and bandwidth-parameterization based controller tuning. In: Proceedings of the 2003 American Control Conference, 2003. pp. 4989–4996. IEEE (2003)
37. Yang, X., Huang, Y.: Capabilities of extended state observer for estimating uncertainties. In: 2009 American Control Conference. pp. 3700–3705. IEEE (2009)
38. Jung, S., Hsia, T.C.: Neural network impedance force control of robot manipulator. IEEE Trans. Ind. Electron. **45**(3), 451–461 (1998). https://doi.org/10.1109/41.679003

Yunfei Dong received the B.S. degree in engineering mechanics from Tsinghua University, Beijing, China, in 2015. He is currently pursuing the Ph.D. degree at Department of Mechanical Engineering, Tsinghua University, Beijing, China. His research interests focus on robot dynamics and force control.

Tianyu Ren received the B.S. degree in mechanical engineering from Beijing Institute of Technology, Beijing, China, in 2014, and the Ph.D. degree in mechanical engineering from Tsinghua University, Beijing, China in 2019. He is currently doing post-doctoral research in Department of Computer Science, Technische Universität Darmstadt, Darmstadt, Germany. His research focuses mainly on robot force control, manipulation and human-robot interaction.

Dan Wu received the B.S., M.S., and Ph.D. degrees in mechanical engineering from Tsinghua University, Beijing, China, in 1988, 1990, and 2008, respectively. She is currently a professor in the Department of Mechanical Engineering, Tsinghua University, Beijing, China and she is a member of American Society for Precision Engineering, and a senior member of the Chinese Mechanical Engineering Society. Her research interests focus on precision and ultra-precision machining, and micro-manipulator for life science. She has authored/coauthored more than 120 research papers, five book chapters, and over 20 granted patents. She won the Science and Technology Progress Award from Ministry of Education of China and the Award of Beijing Higher Education Achievements.

Ken Chen received the B.S. degree in mechanical engineering from Sichuan University, Chengdu, China, in 1982, and the M.S. and Ph.D. degrees in mechanical engineering from Zhejiang University, Hangzhou, China, in 1984 and 1987, respectively. He is currently a professor in the Department of Mechanical Engineering, Tsinghua University, Beijing, China. From 1991 to 1992, he was a Visiting Professor at the University of Illinois, Chicago. From 1992 to 1995, he was a Postdoctoral Researcher with Purdue University, Indianapolis. He has published more than 200 papers. His research interests include bionic-robots, special robots and robotic manufacturing. Prof. Chen is a member of the American Society of Mechanical Engineers, and a senior member of the Chinese Mechanical Engineering Society.